269
10/31/79

LA-7885-MS, Vol. IV

MASTER

LA.210

Informal Report

1-GWh Diurnal Load-Leveling Superconducting Magnetic Energy Storage System Reference Design

Appendix C: Dewar and Structural Support

University of California

LOS ALAMOS SCIENTIFIC LABORATORY

Post Office Box 1663 Los Alamos, New Mexico 87545

LA-7885-MS, Vol. IV
informal Report
UC-20b and UC-94b
Issued: September 1979

1-GWh Diurnal Load-Leveling Superconducting Magnetic Energy Storage System Reference Design

Appendix C: Dewar and Structural Support

J. G. Bennett
F. D. Ju

1-GWh DIURNAL LOAD-LEVELING SUPERCONDUCTING MAGNETIC ENERGY STORAGE SYSTEM REFERENCE DESIGN

APPENDIX C

DEWAR AND STRUCTURAL SUPPORT

BY

J. G. Bennett and F. D. Ju

ABSTRACT

The mechanical aspects of the dewar to contain a 1-GWh superconducting coil in a 1.8 K helium bath and the means for supporting the coil and dewar against the rock of an underground excavation created for just that purpose are presented.

I. INTRODUCTION

Several self-imposed limitations on the 1-GWh Superconducting Magnetic Energy Storage (SMES) components have dictated the preliminary design procedures presented here. Among these limitations is the single-cavity concept and the associated geometric constraint. With the single-cavity concept, the large axial loads near the ends of the solenoid must be taken as a shear load on the rock-cavity walls. For this reason and for reasons of redundancy, the inner helium vessel is segmented. Thus, based on an approximate maximum strain criteria for the high-purity aluminum in the stacked conductors, the conductor-bearing stresses are assumed to accumulate to about 84 MPa (12,200 psi) before transmitting this load to the rock. The vessel is used as structural support for the conductor between the attachment points to the rock.

The design is restricted to commercially available structural materials of common shapes rather than a predication based on a materials development program in "unobtainium." The parameter studies, however, that have led to the design have been quite general with regard to material properties.

Consideration has also been given to construction technology and techniques currently available. The designs considered are buildable with present or easily developed technology.

These combined constraints have dictated that conventional design and analytical methods be utilized. A basic cross section of a 13-segment dewar cavity is shown in Fig. C-1. Dimensions may vary, but they are representative of the 1-GWh concept. Features illustrated in Fig. C-1 are meant to indicate how the component part is or will be designed but are not meant to represent detail.

II. DESIGN OF THE HELIUM VESSEL AS A LOAD-CARRYING MEMBER

A. The Shell Concept

Figure C-2 shows a preformed rippled shell with the inflection point at the point of tangency to the supporting member. A free-body diagram of the shell section from the midspan to the point of tangency at the support, Fig. C-3, allows the following equilibrium equations to be written in terms of the support forces per unit length, $\bar{V}$ and $\bar{S}$, and support moment per unit length, M_s

$$N_{\theta\theta} = \bar{S} \cos \theta + \bar{V} \sin \theta + pR[1 - \cos (\phi - \theta)],$$

$$N_{xx} = N_{x\theta} = 0,$$

$$M_{\theta\theta} = M_s - \bar{S}R(\cos \phi - \cos \theta) - \bar{V}R(\sin \phi - \sin \theta) + pR^2[1 - \cos (\phi - \theta)],$$

and

$$M_{xx} = M_{x\theta} = 0 \quad .$$

Also,

$$\bar{V} = pR \sin \phi \quad ,$$

where p is the pressure loading the shell must carry,

N_{ij} = the shell stress resultants, and

M_{ij} = the shell moment resultants,

all of which are defined with respect to the middle surface of the shell.

An expression is now formed for the complementary energy, U*, per unit length for the cylindrical shell as the membrane plus the bending energy and elastic behavior is assumed.

$$U^* = U = \frac{1}{2Eh} \int_o^{\phi} N_{\theta\theta}^2 R d\theta + \frac{1}{2(1 - \nu^2)D} \int_o^{\phi} M_{\theta\theta}^2 R d\theta \quad ,$$

where

U = the strain energy per unit length of the shell,

E = Young's modulus of elasticity,

h = the shell thickness,

ν = Poisson's ratio, and

$D = \dfrac{Eh^3}{12(1 - \nu^2)}$ = the flexural stiffness of the shell.

Substitution of the expressions for $N_{\theta\theta}$ and $M_{\theta\theta}$ into this expression and performance of the indicated integration gives an equation for U*. Castigliano's theorem[1] is applied to the result.

Because the meridional displacement along the shell arc length is zero at midspan and at the support, then

$$\frac{\partial U^*}{\partial \bar{S}} = 0 \quad .$$

The resulting equation is

$$\frac{1}{12}\left(\frac{h}{R}\right)^2\left[\bar{S}\left(\frac{\phi}{2}+\frac{1}{4}\sin 2\phi\right)+pR\left(\sin\phi-\phi\cos\phi-\frac{1}{4}\cos\phi\sin 2\phi\right)\right]$$

$$+\left[\frac{M}{R}\left(\sin\phi-\phi\cos\phi\right)+\left(\bar{S}-pR\cos\phi\right)\left(\frac{\phi}{2}+\phi\cos^2\phi-\frac{3}{4}\sin 2\phi\right)\right]=0 \quad \text{(C-1)} \ .$$

Also, the slope at the support and at midspan is required to be zero. Therefore,

$$\frac{\partial U^*}{\partial M}=0 \ ,$$

which results in

$$M\phi+\left(\bar{S}-pR\cos\phi\right)\left(\sin\phi-\phi\cos\phi\right)R=0 \ . \qquad \text{(C-2)}$$

By expressing $\bar{S}$ as

$$\bar{S}=pR\cos\phi+\varepsilon S^* \ ,$$

where $\varepsilon=\left(\frac{h}{R}\right)^2$ and p is the radial magnetic pressure, Eqs. (C-1) and (C-2) can be solved for s^* providing all terms of order ε^2 are neglected. Then

$$N_{\theta\theta}=pR\left[1-\frac{\frac{1}{6}\left(\frac{h}{R}\right)^2\phi\sin\phi\cos\theta}{\phi^2+\frac{1}{2}\phi\sin 2\phi-2\sin^2\phi}\right]+O(\varepsilon^2) \qquad \text{(C-3)}$$

and

$$M_{\theta\theta} = \frac{1}{6}\left(\frac{h}{R}\right)^2 p^2R^2 \sin\phi \left(\frac{\sin\phi - \phi\cos\theta}{\phi^2 + \frac{1}{2}\phi\sin 2\phi - 2\sin^2\phi}\right) + O(\epsilon^2) \quad . \qquad \text{(C-4)}$$

Ultimately, the shell will be designed by considering the combined normal stresses, which are maximum at the tangent to the support, that is, $\theta = \phi$. The effects of the axial magnetic loading and cooldown stresses on the vessel design must also be considered. Before considering the vessel as a whole, however, the results thus far obtained, that is, the effects of the radial magnetic loading imposed only on the outer vessel wall, designed as a shell, must be examined.

For a thin shell, the maximum normal hoop stress from combined bending moment and membrane force is approximately

$$\sigma_{\theta\theta} = \frac{N_{\theta\theta}}{h} \pm \frac{6M_{\theta\theta}}{h^2} \quad .$$

For consideration of the magnetic pressure loading only, a stress design requirement can be imposed such that $\sigma_{\theta\theta}{}_{max} \leq \sigma_{design} = 2/3\ \sigma$, where σ is the low temperature yield strength value.

Combining Eqs. (C-3) and (C-4) with $\theta \to \phi$ gives

$$\sigma_{\theta\theta}{}_{max} \leq \frac{pR}{h}\left[1 - \frac{\left(\frac{h}{R}\right)^2 \phi\sin 2\phi}{12f(\phi)}\right] \pm p\left[\frac{\sin\phi\,(\sin\phi - \phi\cos\phi)}{f(\phi)}\right] \quad , \qquad \text{(C-5)}$$

where

$$f(\phi) = \phi^2 + \frac{1}{2}\phi\sin 2\phi - 2\sin^2\phi \quad .$$

If the definitions

$$G(\phi) = \frac{\phi \sin 2\phi}{f(\phi)} \quad ,$$

$$H(\phi) = \frac{\sin \phi \, (\sin \phi - \phi \cos \phi)}{f(\phi)} \quad ,$$

and

$$\sigma_A = \sigma_{\substack{\theta\theta \\ max}} = \text{allowable stress in the shell}$$

are used, Eq. (C-5) can be rewritten as

$$\sigma_A = \frac{pR}{h} \left\{ 1 - \frac{1}{12} \left(\frac{h}{R}\right)^2 G(\phi) \right\} \pm pH(\phi) \quad . \qquad \text{(C-6)}$$

This equation can now be solved for $h(R,\phi)$, the shell thickness. Because the first term in Eq. (C-6) is positive for positive pressure and is the membrane stress and the second term is the bending contribution, to insure the maximum stress is used, the sum of the membrane and absolute values of the bending stress are combined to give

$$h(R,\phi) = \frac{-\sigma_A + |pH(\phi)| + \left([\sigma_A - |pH(\phi)|]^2 + \frac{p^2 G(\phi)}{3} \right)^{1/2}}{\frac{pG(\phi)}{6R}} \quad . \qquad \text{(C-7)}$$

Thus far, no geometric constraint has been incorporated into Eq. (C-7). For a given geometric configuration, Fig. C-2, the support spacing s, half-angle ϕ, shell unsupported radius of curvature R, and support radius r, are related by

$$s = 2(R + r) \sin \phi \quad .$$

Let $\eta = \frac{r}{R}$, so that

$$\phi = \sin^{-1}\left(\frac{s}{2R(1+\eta)}\right) \quad . \tag{C-8}$$

For a given design, Eqs. (C-7) and (C-8) must be satisfied simultaneously. To see the influence of various parameters on shell thicknesses and volume, the parameters in Eq. (C-7) will be varied and Eq. (C-8) will be plotted over the result for a specific value of η. This graphical solution gives a good method for examination of the effect of changing the parameters for a specific design.

The total shell volume can be shown to be

$$V = \pi DHh(R,\phi)\,\frac{\phi}{\sin\phi} \quad ,$$

where

D = the coil diameter and

H = the shell height.

Figures C-4 and C-5 illustrate typical parameter studies, where the following parameters representative of a typical end segment in the multisegmented dewar concept were used.

SMES diameter D = 132 m

Shell height H = 2 m

Radial magnetic pressure p' = 20.7 MPa

Material properties used = A304-LN austenetic stainless steel

Allowable stress σ_A = 510 MPa

Young's modulus of elasticity, E = 20.7 GPa

$\eta = r/R = 0.55$

Figure C-4 shows the shell thickness of Eq. (C-7) solved for various half-angles ϕ and ripple radii R. As can be seen, as the half-angle becomes small, the thickness increases rapidly to accommodate the increased bending stresses at the support point of tangency. The geometric constraints for

potential vessel geometries, Eq. (C-8), are shown for three support spacings and for $\eta = 0.55$ on Fig. C-4.

Figure C-5 shows the same study with $V(R, \phi)$, the shell volume, plotted. Note that the volume function shows a slight minimum at around $\phi = 30^{\circ}$. Study of both figures indicates that larger half-angles are beneficial in reducing the shell thickness and volume.

One should not be confused by Figs. C-4 and C-5. Their potential usefulness may be seen by considering a specific example.

Let

$$r = 0.5 \text{ m}$$

and

$$\frac{r}{R} = 0.55 \rightarrow R = 0.91 \text{ m};$$

for

$$s = 2 \text{ m and}$$

$$\phi = \sin^{-1}\left(\frac{2}{2(1 + 0.55)0.91}\right) = 45.2^{\circ} \quad ,$$

then from Fig. C-4 $h \simeq 0.25$ cm and from Fig. C-5 $V \simeq 0.7$ m.

The value of $\eta = r/R = 0.55$ requires a 0.7-m length of shell to be supported. This length of support does not lead to a reasonable design. The trends for all values of η will be the same.

Figures C-4 and C-5 are not restricted to $\eta = 0.55$. One further example will illustrate this point.

Let

$r = 0.2$ m,

$s = 2$ m,

and

$\phi = 30^{\circ}$;

then from the geometric constraint Eq.(C-8),

$R = 1.8$ m and

$\eta = 0.11$.

From Figs. C-4 and C-5,

$h \simeq 1$ cm

and

$V \simeq 1.8$ m^3.

If desired, the curves for $\eta = 0.11$ and $s = 2$ m can be plotted over Figs. C-4 and C-5. By this example, one point has been located on the curve.

These examples are given to illustrate the meaning of Figs. C-4 and C-5, not to imply their utility as design tools. Their real value is to examine the effect that the various parameters have on the shell thickness and volume.

It is clear from a study of Figs. C-4 and C-5 that closely spaced supports, implying less unsupported span, are also a means of reducing shell volume, particularly for smaller half-angles. Costwise, structural material is moved from the shell to the support, and the total material cost will depend on the relative cost of support material as compared with shell material.

For higher values of half-angle, the geometric constraint curves of Figs. C-4 and C-5 come together for large values of ϕ and the trade-off of shell material for support material is not as important. The advantage of the wider support spacing is in having room available for ease in construction and final assembly in the tunnels. A support spacing of about 2 m on centers is judged to be about minimum for assembly without having to resort to unconventional construction techniques.

B. Cooldown Stresses in the Rippled Shell

Consider the cooldown of the preformed rippled shell structure anchored periodically as shown in Fig. C-2. The shell will not shrink freely upon cooling because of the anchor constraints. The membrane forces and couples that will occur as the shell is cooled will cause a flattening and stretching of the shell. Furthermore, if the shell can unwrap from the support at point C of Fig. C-2, these stresses will be different from the case for which point C is constrained to remain in contact with the support.

The assumption is made that at point A the displacement and slope of the shell are constrained to remain zero. From this assumption the case for which unwrapping can occur is formulated. The resulting equations can be reduced to the case for which point C remains in contact with the support with zero slope by letting r, the support radius of curvature, approach zero.

Mathematical Model

Because of the symmetrical condition, only a section of the shell needs to be considered. Figure C-6 shows the section AB where A is the anchor point such that there is no displacement nor rotation thereof. The point B is the symmetrical point, where the continuity conditions for displacement and slope require that the lateral displacement be equal to the lateral thermal contraction and that the slope is zero. The point C is a functionally discontinuity point.

Figure C-6 shows the free-body diagram for the formulation. The membrane complementary energy of order $(h/R)^2$, as compared to the bending complementary energy, is assumed to be negligible. The material is assumed to be linearly elastic, and the energy equation is written as

$$U^* = U = \frac{1}{2(1 - \nu^2)D} \int_S M(s)^2 \, dS \ , \tag{C-9}$$

where

$M(s)$ = the moment function along the arc lengths, s,

$D = \dfrac{Eh^2}{12(1 - \nu^2)}$ = the shell flexural stiffness,

ν = Poisson's ratio,

U^* = the complementary energy per unit shell length, and

U = the strain energy per unit shell length.

For the free-body diagram in Fig. C-6, the following equations of equilibrium can be written for $0 \leq \theta \leq \phi$ and S between B and C,

$$M(s) = - M_B + P_B(1 - \cos \theta)R + Q_B R \sin \theta \ , \tag{C-10}$$

and for $0 \leq \theta \leq \phi$ and S between A and C ,

$$M(s) = - M_B + P_B \left[R(1 - \cos \phi) + r(\cos \theta - \cos \phi)\right] + Q_B \left[R \sin \phi + r(\sin \phi - \sin \theta)\right] \ , \tag{C-11}$$

where Q_B is zero from symmetry considerations. The Q_B is kept, however, to determine the displacement in the direction of Q_B at position B.

Equations (C-9), (C-10), and (C-11) can be used to apply Castigliano's theorem.[1] Because all static constraints have corresponding zero slopes and

displacements, they are nonworking and the classical Castigliano's theorem results.

$$\left.\frac{\partial U}{\partial M_B}\right|_{Q_B=0} = \Delta\theta_B = 0 \quad , \tag{C-12}$$

$$\left.\frac{\partial U}{\partial P_B}\right|_{Q_B=0} = \delta P_B = (R + r)\,\varepsilon_T \sin\phi \quad , \tag{C-13}$$

and

$$\left.\frac{\partial U}{\partial Q_B}\right|_{Q_B=0} = \delta Q_B \quad , \tag{C-14}$$

where ε_T is the total thermal strain over the temperature range of cooldown.

Performing the operations indicated by Eqs. (C-12), (C-13), and (C-14) on Eqs. (C-9), (C-10), and (C-11) will give two equations that can be solved for unknowns M_B and P_B and one equation for δQ_B involving M_B and P_B. The quantities of interest are given here as the membrane force and couple at B.

$$P_B = \frac{Eh^3}{12R^2}\,\varepsilon_T\,\frac{\sin\phi}{\bar{f}(\phi)} \tag{C-15}$$

and

$$M_T = \frac{Eh^3}{12R}\,\varepsilon_T\,\sin\phi\,\frac{\left[1 - \left(1 - \frac{r}{R}\right)\frac{\sin\phi}{\phi} - \frac{r}{R}\cos\phi\right]}{\bar{f}(\phi)} \quad , \tag{C-16}$$

where

$$\bar{f}(\phi) = \frac{\phi}{2}\left(1 - \frac{r^2}{R^2}\right) + \frac{r}{R}\frac{\phi}{2}\cos 2\phi$$

$$+ \frac{1}{4}\sin 2\phi\left(1 - 5\frac{r}{R} + \frac{r^2}{R^2}\right) - \left(1 - \frac{r}{R}\right)^2 \frac{\sin^2\phi}{\phi} \quad . \qquad \text{(C-17)}$$

Also, from symmetry and equilibrium considerations

$$Q_A = Q_B = 0 \quad ,$$

$$P_A = P_B \quad ,$$

and

$$M_B = \frac{Eh^3}{12R}\varepsilon_T \sin\phi \left[\frac{\frac{r}{R} + \left(1 - \frac{r}{R}\right)\frac{\sin\phi}{\phi} - \cos\phi}{\bar{f}(\phi)}\right] \quad . \qquad \text{(C-18)}$$

The maximum tensile stress will occur at A and for small h/R. This stress can be expressed as

$$\sigma_{\theta\theta} = \frac{P_A}{h} + \frac{6M_A}{h^2}$$

or

$$\sigma_{\theta\theta} = \frac{Eh\varepsilon_T \sin\phi}{12R\bar{f}(\phi)}\left[\frac{h}{R} + 6\left(\frac{r}{R} + \left(1 - \frac{r}{R}\right)\frac{\sin\phi}{\phi} - \cos\phi\right)\right] \quad . \qquad \text{(C-19)}$$

To examine the effects of cooldown alone on the shell, Eq. (C-19) is evaluated for the following geometric parameters.

$$\eta = \frac{r}{R} = 0.25$$

and

$$S = \text{the support spacing} = 2 \text{ m} \quad ,$$

and for the material properties of steel and aluminum,

$$E_{STEEL} = 208 \text{ GPa} \quad ,$$

$$E_{ALUMINUM} = 73 \text{ GPa} \quad ,$$

$$\varepsilon_{T\text{-}STEEL} = 2.96 \times 10^{-3} \quad ,$$

and

$$\varepsilon_{T\text{-}ALUMINUM} = 4.15 \times 10^{-3} \quad .$$

Average values of ε_T are chosen for cooldown from 273 to 0 K.

Table C-I gives the results for various thicknesses h and half-angles ϕ. Table C-I reflects the fact that for aluminum, the total thermal strain increases by about 1.4 times, whereas the elastic modulus is about one-third that of steel. This results in an overall thermal stress reduction of about one-half for aluminum over that for steel. Table C-I also illustrates two geometric effects. First, increasing the half-angle decreases the magnitude of the cooldown stresses for the so-called "straightening out" effect. Second, increasing the thickness increases the magnitude of the cooldown stresses for the stiffening effect.

TABLE C-I

MAXIMUM STRESS AT POSITION A IN MPa

	Thickness h (m)					
	Steel			Aluminum		
ϕ°	0.01	0.02	0.03	0.01	0.02	0.03
20	88.9	180.5	274.8	43.8	88.9	135.4
25	69.6	141.0	214.1	34.3	69.5	105.5
30	56.7	114.5	173.5	27.9	56.4	85.5
35	47.3	95.4	144.4	23.3	47.0	71.1
40	40.1	80.9	122.2	19.8	39.8	60.2
45	34.4	69.3	104.7	17.0	34.2	51.6
50	29.8	60.0	90.5	14.7	29.5	44.6
90	10.0	20.1	30.3	4.9	9.9	14.9

To convert the above values to psi, multiply by 145.04.

These results are intended to illustrate the effects of cooldown and to show that the stresses must be accounted for in the design. In the analysis presented, the shell is assumed to be able to unwrap from the support. The construction of the dewar will be simplified if supports are put in place first and then the shell is attached between the adjacent supports. This design is the nonunwrapping case analyzed in a previous section with pressure loading. The present thermal stress analysis reduces to this case if $r \to 0$ in Eqs. (C-17) and (C-19). Equation (C-19) becomes

$$\sigma_{\theta\theta} = \frac{Eh\epsilon_T \sin \phi}{2R\bar{f}(\phi)} \left[\frac{h}{R} + 6 \left(\frac{\sin \phi}{\phi} - \cos \phi\right)\right] \tag{C-20}$$

and Eq. (C-17) now becomes

$$\bar{f}(\phi) = \frac{\phi}{2} + \frac{\sin 2\phi}{4} - \frac{\sin^2 \phi}{\phi} \tag{C-21}$$

and

$$2\phi\bar{f}(\phi) \approx f(\phi) \quad ,$$

with $f(\phi)$ as defined previously for Eq.(C-5). The combined radial pressure loading and cooldown stresses can now be examined.

C. Shell Stresses from Combined Cooldown and Radial Magnetic Pressure Loading

Equations (C-6) and (C-20) can be combined with attention given to the signs from the free body diagrams to give the following result:

$$\sigma_{\theta\theta} = \frac{pR}{h}\left\{1 - \frac{h^2}{12R^2}\,G(\phi)\right\} + \frac{Eh\varepsilon_T \sin\phi}{12R\,\bar{f}(\phi)}\left(\frac{h}{R}\right)$$

and

$$+ \text{ABS}\left\{\frac{Eh\varepsilon_T \sin\phi}{12R\,\bar{f}(\phi)}\,6\left(\frac{\sin\phi}{\phi} - \cos\phi\right) - pH(\phi)\right\} \quad . \qquad (C\text{-}22)$$

where the result has not been simplified to identify the terms physically. Equation (C-22) is the equation for the maximum stress from combined cooldown and pressure loading in the shell at point C in Fig. C-2. The first term represents the membrane stress in the shell that arises because of the pressure loading. Note the appearance of the expected pR/h term plus a geometric correction. The second term is the membrane stress that arises from cooldown. The first half of the third term is the bending cooldown stress, and the last half of the third term is the bending stress caused by the pressure. The absolute value of both bending contributions is taken to insure that the maximum tensile stress is obtained. Because of the different positive bending moments assumed in the derivations, the difference between these bending terms must be used. Physically, this is indicative of the fact that the bending because of cooldown is somewhat reduced by applying the

pressure. Both the thermal and pressure loadings produce membrane tensions that are additive.

Equation (C-22) has been studied parametrically to determine if an optimum shell design can be achieved. For this study, the value of support spacing s was held constant at 2 m and support radius r at 0.2 m. For a given unsupported radius, R, the half-angle is then fixed by Eq. (C-8). Figure C-7 shows the surface that results from plotting $\sigma_{\theta\theta}$ versus 1/R versus h under the above constraints.

It is interesting to note that the surface exhibits a saddle point for small values of 1/R. In general, the trends noted from the two previous studies are also clearly evident here. The stresses decrease with increasing unsupported curvature and initially decrease as the thickness is increased; however, because the thermal bending strain begins to dominate for very thick members, the stress correspondingly increases. There does not appear to be a curvature that will give a minimum volume; but once the curvature is selected, there is a thickness that will give a minimum stress. The minimum volume will be given by the minimum thickness corresponding to the design stress and the specified unsupported curvature. The conclusion of this study is that the half-angle and curvature should be picked to correspond with ease of construction and to be large enough to reduce the maximum stress below the design stress. A study of the data reveals that for a radial pressure loading of 2.07 MPa, a 2-m support spacing, and a 0.2-m support radius, a minimum half-angle of about 16° with a maximum unsupported radius of curvature of around 3 m is required to reduce the maximum stress to around 520 MPa. In the 1-GWh SMES, radial pressures are between 2.5 and 5.7 MPa so that rather large unit half-angles will be required.

All studies thus far have been to determine the boundaries of the design. The vessel must also carry the axial component of the magnetic loading between supports. To investigate the final design, the resultant axial magnetic loading is included. This loading is assumed to be carried by the vessel acting as a beam between supports.

D. Closed Helium Vessel Design Considerations

Consider the cross section shown in Fig. C-8. The segmented dewar sections are designed based on this cross section. The requirement that the outer wall will act as a shell as far as the radial component of the magnetic

loading is concerned will mean that a certain amount of stand-off distance, which will be at least one-tenth the unsupported radius of curvature, will be required for the conductors from the top and bottom closures and from any cross shear connections. The inner wall carries only the helium hydrostatic pressure radially and could be very thin except that the inner wall also acts as a shear web member for the vessel acting as a beam.

Three assumptions are made. These are (1) that the interior of the vessel is filled with the conductors and cooling channels with the remaining space filled with material such as plastic where needed for spacing and load transfer purposes, (2) that based on an approximate strain limit in the conductors, the stress in the conductors is allowed to accumulate to about 105 MPa before carrying the load to the vessel walls, and (3) that stability of the walls exists against any web deformation.

Based on field calculations, the 13-segment helium vessel will carry a vertical load component of about 21 MN/m of peripheral length. Because the vessel is continuous, the maximumm direct shear force, V, and the bending moment, M, at the support can be written as

$$V = \frac{w\ell}{2}$$

and

$$M = \frac{w\ell^2}{12} \quad ,$$

where w is the vertical load per unit length. The combined stresses from all effects have been investigated both at the support and the midspan where the thermal effects are all additive. The stresses have always been found to be a maximum at the support at location A of Fig. C-8. A differential element at location A of Fig. C-7 is assumed to be stressed as shown in Fig. C-9, where $\sigma_{\theta\theta}$ = the shell stress from the radial magnetic and thermal loading, σ_{zz} = the bending stress from the axial magnetic loading (support moment), and τ_{xz} = the shear stress from the axial magnetic loading (direct shear).

The design is based on the principal stress computed from the assumed stress distribution at A being less than the design stress, which is taken to

TABLE C-II

LOW-TEMPERATURE DESIGN PARAMETERS

	Aluminum Alloy	Steel A304-LN
Yield strength, MPa	414	771
Stress, MPa	276	517
Shear, MN	20	20
Moment, MN-m	6.32	6.32
Thermal strain, ε_T	4.15×10^{-3}	2.97×10^{-3}
Material cost \$/m^3	\$4 880	17 300
\$/lb	0.80	1.00

be two-thirds the low-temperature yield value of the material. The parameters in Table C-II are pertinent with regard to the results presented.

The design shear and moment values vary with geometry. The values quoted in Table C-II are for the case of a support radius of curvature of 0.2 m, unsupported radius of curvature of 1.8 m, half-angle of 45°, and support spacing of 2 m.

To examine the effects of the various contributions of each component to the stresses on Element A, two identical geometries for the aluminum and steel were constructed. Figure C-10 shows typical curves obtained for maximum principal stress versus outer wall thicknesses for two closure thicknesses. Figure C-11 shows a typical result from a point comparison. As can be seen from Fig. C-11, the only components of stress affected by the material properties are those contributions from the thermal effects. Note that the thermal effects in the aluminum are less predominant.

Note also that for this particular geometry the maximum principal stress in the aluminum is above the design stress while that for the steel is below. For a given geometry, the stresses in the aluminum can be decreased by increasing wall thicknesses until thermal effects begin to dominate and then by increasing the top and bottom closure thicknesses to reduce the bending and shear stress contribution. Attempts to find a reasonable design for aluminum for the 2-m support spacing lead to extremely thick designs and technological problems in field welding and construction. The alternative is to reduce the

support spacing and thus the loadings. The economic trade-off is vessel material for support material. This trade-off should be investigated in the future because of the very attractive unit price of aluminum as opposed to steel. See Table C-II. At this time, however, no futher consideration is given to the aluminum vessel design.

Tables C-III and C-IV give the sizes of a typical 13-segment and 25-segment dewar design of A304-LN austenetic stainless steel. All vessel widths were taken to be 0.1 m. Although there appears to be some economic advantage in keeping the segments as tall as possible, the additional internal structure required to transfer the load to the bottom of the vessel may offset some of the apparent savings. These comparisons are given to show how to proceed toward an optimized cost design once a specific reference point has been established.

For comparison, Table C-V gives the sizes of a 25-segment design for aluminum. The evident saving in material cost provides a strong incentive for developing the technology for field welding of thick aluminum sections.

TABLE C-III

A304-LN STAINLESS STEEL 13-SEGMENT VESSEL

		Vessel Geometry(w = 0.1 m)							Single Segment Volume of Material	Costs 10^6	
Segment Number	Radial Design Pressure MPa	R m	r m	H m	ϕ deg	h_1 cm	h_t^* cm	h_s cm	m^3	Single Segment	Total
1 & 7	2.5	1.21	0.2	2.2	45	1.0	2.0	1.6	27.6	0.48	0.96
2 & 8	3.7	1.21	0.2	1.7	45	1.0	9.2	3.4	39.2	0.68	1.36
3 & 9	4.0	1.21	0.2	1.8	45	1.0	7.2	3.1	37.7	0.65	1.30
4 & 10	4.7	1.21	0.2	2.0	45	1.0	5.2	2.8	37.9	0.66	1.31
5 & 11	5.4	1.21	0.2	2.3	45	1.0	3.8	2.5	39.7	0.69	1.37
6 & 12	5.5	1.21	0.2	2.9	45	1.0	2.4	2.0	42.0	0.73	1.45
13	5.7	1.21	0.2	18.2	45	1.0	1.0	1.4	203.7	33.52	3.52
									Total	11.3×10^6	

*$h_t = h_b$

TABLE C-IV

A304-LN STAINLESS STEEL 25-SEGMENT VESSEL

Segment Number	Radial Design Pressure MPa	Vessel Geometry(w = 0.1 m) R m	r m	H m	φ deg	h_i cm	h_t^* cm	h_s cm	Single Segment Volume of Material m^3	Costs $10^6 Single Segment	Costs $10^6 Total
1,2,13,14	2.5	1.21	0.2	1.46	45	1.0	3.2	1.6	19.4	0.34	1.34
3,4,15,16	3.7	1.21	0.2	1.21	45	1.0	7.6	2.6	24.6	0.43	1.70
5,6,17,18	4.0	1.21	0.2	1.26	45	1.0	5.4	2.8	24.9	0.43	1.72
7,8,19,20	4.7	1.21	0.2	1.36	45	1.0	5.4	2.6	25.9	0.45	1.79
9,10,21,22	5.4	1.21	0.2	1.51	45	1.0	5.4	2.5	27.6	0.48	1.91
11,12,23,24	5.5	1.21	0.2	1.81	45	1.0	3.2	2.2	28.5	0.49	1.97
25	5.7	1.21	0.2	18.2	45	1.0	1.0	1.4	203.7	3.52	3.52
									Total	$14.0×10^6	

*$h_t = h_b$

TABLE C-V

ALUMINUM 25-SEGMENT VESSEL

Segment Number	Radial Design Pressure MPa	Vessel Geometry(w = 0.1 m) R m	r m	H m	φ deg	h_i cm	h_t^* cm	h_s cm	Single Segment Volume of Material m^3	Costs $10^6 Single Segment	Costs $10^6 Total
1,2,13,14	2.5	1.21	0.2	1.46	45	1.0	13.7	2.27	31.0	0.151	0.605
3,4,15,16	3.7	1.21	0.2	1.21	45	1.0	23.5	3.22	36.0	0.176	0.703
5,6,17,18	4.0	1.21	0.2	1.26	45	1.0	22.5	3.55	37.7	0.184	0.736
7,8,19,20	4.7	1.21	0.2	1.36	45	1.0	25.3	3.65	41.6	0.203	0.812
9,10,21,22	5.4	1.21	0.2	1.51	45	1.0	25.3	3.97	46.3	0.226	0.904
11,12,23,24	5.5	1.21	0.2	1.81	45	1.0	17.9	3.96	49.7	0.243	0.970
25	5.7	1.21	0.2	18.2	45	1.0	1.0	2.58	302.5	1.48	1.48
									Total	$6.21×10^6	

*$h_t = h_b$

E. The Box-Beam Concept

An alternate approach for the helium vessel is to design the cross section as a box beam with methods similar to those used for aircraft wings. The results of this section can also be used to estimate the stresses in the vessel of the previous section for the ring at the upper and lower closures. The potential for designing the conductors as load-carrying members has also been included in the formulation so that such a design could be studied.

F. Formulation of the General Problem

Figure C-12 shows a cross section between supports of the most general geometry considered. Figure C-13 shows a typical helium vessel segment cross section to which the formulation can apply.

The support is assumed to be elastic; and the beam is divided into two regions, supported and unsupported, as in the shell formulation. In this manner, the same cases are treated for the shell. Also an additional consideration of a possible elastic support is included if different geometric and material properties are maintained in each region.

Figures C-14 and C-15 show the n-th radial beam segment and the effects considered in each region. Constant curvatures are assumed in each region. The interface pressures in each region are assumed to be uniform to correspond to uniform magnetic loading in each region. If the equations are formulated for solution to the beams as shown, then both the conductor-beam and dewar-beam interactions can be studied. The equations for each beam are assembled into a matrix form, and displacements at their midspan are made compatible.

From a free-body diagram of the n-th unsupported region for $0 < \psi < \phi$ of Fig. C-16, the following equations of equilibrium can be written.

$$M(\psi) = M_\phi + F_R R_n \sin^2\left(\frac{\psi}{2}\right) + R_\phi R_n \sin\psi - 2T_\phi R_n \sin^2\left(\frac{\psi}{2}\right) ,$$

$$T(\psi) = F_R \sin^2\left(\frac{\psi}{2}\right) + R_\phi \sin\psi + T_\phi \cos\psi , \qquad \text{(C-23)}$$

and

$$V(\psi) = \frac{1}{2} F_R \sin \psi - T_\phi \sin \psi + R_\phi \cos \psi \quad ,$$

where

R_ϕ = a ficticious load normal to the beam introduced at $\phi = 0$,

M_ϕ = the resultant moment at $\phi = 0$,

T_ϕ = the resultant beam axial force at $\phi = 0$,

$M(\psi)$ = the resultant moment at ψ,

$T(\psi)$ = the resultant beam axial force at ψ,

$V(\psi)$ = the resultant beam direct shear force at ψ,

$$F_R = 2p_n^{(n-1)}(R_n - t_n) + 2p_n^{(B)}R_n - 2p_n^{(n+1)}(R_n + t_n),$$

$p_i^{(i+1)}$ = the force per unit length on the i-th beam caused by the (i + 1)-th,

$p_i^{(B)}$ = the force per unit length on the i-th beam caused by the radial component of the magnetic field,

t_n = the half thickness of the n-th beam, and

R_n = the beam radius of curvature.

From the free-body diagram of the n-th beam in Fig. C-17, the following equilibrium equations can be written for the supported region $0 < \theta < \phi$.

$$M(\theta) = M_\phi - \mathcal{F}_r r_n \sin^2\left(\frac{\theta}{2}\right) \quad A(\phi)F_R - \frac{1}{2} F_R r_n \sin\phi \sin(\phi - \theta)$$

$$+ F_R r_n \sin^2\left(\frac{\phi}{2}\right) \cos(\phi - \theta) + B(\phi)R_\phi - R_\phi r_n \sin(\phi - \theta)$$

$$- C(\phi)T_\phi - T_\phi r_n \cos(\phi - \theta) \quad ,$$

$$T(\theta) = F_R \left\{\frac{1}{2} \sin\phi \sin(\phi - \theta) - \sin^2\left(\frac{\phi}{2}\right) \cos(\phi - \theta)\right\}$$

$$+ T_\phi \cos(\phi - \theta) + R_\phi \sin(\phi - \theta) + \mathcal{F}_r \sin\left(\frac{\theta}{2}\right)$$

$$\times \left[\sin\left(\phi - \frac{\theta}{2}\right) \cos(\phi - \theta) - \cos\left(\phi - \frac{\theta}{2}\right) \sin(\phi - \theta)\right] \quad , \qquad \text{(C-24)}$$

$$V(\theta) = F_R \left[\sin^2\left(\frac{\phi}{2}\right) \sin(\phi - \theta) + \frac{1}{2} \sin\phi \cos(\phi - \theta)\right]$$

$$- \mathcal{F}_r \sin\left(\frac{\theta}{2}\right) \left\{\sin\left(\phi - \frac{\theta}{2}\right) \sin(\phi - \theta) + \cos\left(\phi - \frac{\theta}{2}\right) \cos(\phi - \theta)\right\}$$

$$+ R_\phi \cos(\phi - \theta) - T_\phi \sin(\phi - \theta) \quad ,$$

and where $\mathcal{F}_r = F_n^{(n+1)}(r_n - t_n) - p_n^{(B)} r_n - {}_n^{(n-1)}(r_n + t_n)$,

$F_n^{(n+1)}$ = the force per unit length in the support region on the n-th beam caused by the (n + 1)-th, and

r_n = the beam radius of curvature in the support region.

The usual strain energy expression in the beam is formed by

$$U = \int_{\ell_1} \frac{M^2(\psi)d\ell_1}{2EI} + \int_{\ell_1} \frac{\alpha^2 V^2(\psi)}{2AG} d\ell_1 + \int_{\ell_1} \frac{T^2(\psi)d\ell_1}{2AE}$$

$$+ \int_{\ell_2} \frac{M^2(\psi)d\ell_2}{2E_s I_s} + \int_{\ell_2} \frac{\alpha^2 V^2(\theta)}{2A_s G_s} d\ell_2 + \int_{\ell_2} \frac{T^2(\theta)d\ell_2}{2A_s E_s} \quad , \qquad \text{(C-25)}$$

where

U = strain energy in the beam,

$d\ell_1 = Rd\psi$,

α = geometric shear stress correction factor,

$d\ell_2 = rd\theta$,

E = Young's modulus of elasticity,

G = shear modulus of elasticity,

A = cross sectional area,

I = moment of inertia about the centroidal bending axis of the beam,

and the subscript, s, denotes the possibility of having different properties in the supported region.

Because of the possible relative shortness of the beam segment as compared with the beam thickness for the vessel, the effects of direct shear deformation have been included in the strain energy expression.

For elastic behavior, Castigliano's theorem[1] can be applied in the following manner. (1) From symmetry requirements on axial displacement at $\psi = 0$ and $\theta = \phi$,

$$\frac{\partial U^*}{\partial T_\phi}\Big|_{R_\phi=0} = \frac{\partial U}{\partial T_\phi}\Big|_{R_\phi=0} = 0 \quad , \qquad \text{(C-26)}$$

where U* is the complementary energy stored in the beam.

The result of carryimg out the operations implied by Eqs. (C-26) and (C-23) for the equilibrium Eqs. (C-24) and (C-25), can be written as

$$A(\phi)M_\phi + B(\phi)T_\phi + C(\phi)F_R + D(\phi)\mathcal{F}_r = 0 \quad . \tag{C-27}$$

(2) From the symmetry requirements on the slope of the beam axis,

$$\frac{\partial U^*}{\partial M_\phi}\Big|_{R_\phi=0} = \frac{\partial U}{\partial M_\phi}\Big|_{R_\phi=0} = 0 \quad ,$$

which gives

$$E(\phi)M_\phi + F(\phi)T_\phi + G(\phi)F_R + H(\phi)\mathcal{F}_r = 0 \quad . \tag{C-28}$$

(3) For assumed zero displacement normal to the beam at $\theta = \phi$, the center of span displacement normal to the beam, u, at $\psi = 0$ can be written as

$$u = \frac{\partial U^*}{\partial R_\phi}\Big|_{R_\phi=0} = \frac{\partial U}{\partial R_\phi}\Big|_{R_\phi=0} \quad , \tag{C-29}$$

which gives

$$u = W(\phi)M_\phi + A(\phi)T_\phi + Y(\phi)F_R + Z(\phi)\mathcal{F}_r \quad . \tag{C-29}$$

Using $\mathcal{F}_r = F_R$ and solving Eqs. (C-27) and (C-28) simultaneously gives

$$M_\phi = P(\phi)F_R \quad ,$$

$$T_\phi = Q(\phi)F_R \quad , \tag{C-30}$$

and Eq. (C-29) as

$$u = Y(\phi)F_R + Z(\phi)\mathcal{F}_r + [W(\phi)P(\phi) + X(\phi)Q(\phi)]F_R \quad . \tag{C-31}$$

All the equations can be written for each beam. To maintain the most flexibility for studying the conductor-vessel system, the equations can be solved numerically. The details are relatively straightforward, and Eq. (C-31) for each beam can be assembled in the form

$$[A]\{x\} = \{B\} \quad , \tag{C-32}$$

where

$$\{x\} = \{u, p_1^{(2)}, p_2^{(3)}, p_3^{(4)} \cdots p_{n-2}^{(n-1)}, p_D^{(n-1)}, F_1^{(2)} \cdots F_D^{(n-1)}\}^T \quad ,$$

and where the following assumptions are used:

$$p_D^{(n-1)} = N_{cv} p_n^{(n-1)},$$

$$F_D^{(n-1)} = N_{cv} F_n^{(n-1)} \quad , \tag{C-33}$$

and

N_{cv} = the number of conductors stacked vertically on the dewar. Note that in writing Eq. (C-33), the assumption is made that radial magnetic loading in the vertical stack can be approximated with a uniform load distribution. Enforcing compatibility at the midspan allows Eq. (C-32) to be solved for the vector {x}. Once the innerface pressures are known, Eq. (C-30) can be solved for the moment and axial load in each beam.

This model attempts to keep all important effects without resulting in excessively large systems of equations or long computational times.

G. Thermal Effects

Once expressions are obtained for the strain energy in the beam, the effects of cooldown follow the same development as for the doubly curved shell. Figure C-18 shows the cooldown kinematics involved. Application of Castgliano's theorem [1] gives

$$\frac{\partial U^*}{\partial M_\phi} = 0 \quad ,$$

$$\frac{\partial U^*}{\partial T_\phi} = (R + r) \sin \phi \varepsilon_T ,$$

and

$$\frac{\partial U^*}{\partial R_\phi} = dy_T \quad ,$$

where dy_T is the midspan displacement normal to the beam. The first two relationships yield equations that can be solved for unknowns M_ϕ and T_ϕ, and then the third can be solved for the midspan displacement.

H. Typical Results from Box-Beam Studies

A number of studies were conducted with a computer code to evaluate numerically the model described. All of these studies attempted to maintain relatively straight beam segments because of the difficulty that would be involved in construction of a highly curved cross section.

The main problem that arises when relatively straight members are considered is the large thermal stresses in the stiff vessels. Table C-VI gives the design parameters used to generate Figs. C-19 and C-20. These parameters are typical of those for a helium vessel end segment. Figure C-19 shows the cooldown stresses in a box-beam steel vessel as a function of the unsupported radius of curvature.

TABLE C-VI

BOX-BEAM DESIGN PARAMETERS FOR FIGS. C-19 AND C-20.

Vessel	
Material	Steel
Young's modulus, GPa	207
Poisson's ratio	0.3
Coefficient of thermal expansion, K^{-1}	1.01×10^{-5}
Cross-sectional moment of inertia, m^4	3.68×10^{-3}
Cross-sectional area, m^2	5.9×10^{-2}
Height, m	2.0
Width, m	0.11
Conductor	
Material	Copper/aluminum
Young's modulus, GPa	138
Poisson's ratio	0.27
Coefficient of thermal expansion, K^{-1}	1.1×10^{-5}
Cross-sectional moment of inertia, m^4	1.7×10^{-10}
Cross-sectional area, m^2	5.9×10^{-2}
Number of conductors radially	5
Number of conductors stacked vertically	20
Geometry	
Support spacing, m	2
Support radius of curvature, m	0.5
Unsupported radius of curvature, m	1000→4
Half-angle, degrees	0.05→12.7

As 1/R approaches zero, the maximum stress is observed to approach the value for a rod clamped between supports, that is, $\sigma = E\varepsilon_T$. As 1/R is increased, thus increasing the half-angle and the depth of the ripple, the maximum stress increases slightly because there is some curvature and the bending stress increases; but there is not enough curvature to allow the straightening effect to relieve the axial stress. As 1/R is increased even

further, the beam can straighten and the maximum stress decreases. Note that when 1/R is 0.25, the stress has decreased to about 390 MPa, a value that is still rather large. For this case the half-angle is about 12.7°, and the beam is no longer considered straight enough to be easily constructed.

The difficulty of constructing a highly curved complex cross section as shown in Fig. C-12 means that the box-beam concept is of questionable value. Simple cross sections as shown in Fig. C-7 and flexible conductors should be more easily constructed. To see the desired effect of increasing curvature, consider the calculated maximum stresses in the comparatively flexible conductor, shown in Fig. C-20. As 1/R increases, the flexible conductor straightens readily and relieves the thermal stresses.

III. SUPPORT STRUT STRUCTURE-HELIUM VESSEL TO ROCK WALL

A. Tunnel Bridge Concept

Several support concepts were investigated. The concept of using both walls of the rock tunnel to carry a portion of the magnetic loading is appealing from the rock mechanics point of view. Figure C-21 shows schematically the basic concept. Axial load components are supported off both walls while radial components are carried only to the outer wall. In this concept, the axial loads are allowed to accumulate in the vessel-conductor structure to 21.1 MN/m before segmenting the dewar and carrying this component to the rock. The axial support struts are visualized as a series of hinged plates 1 m wide and 2 m on centers that bridge the tunnel. The radial supports are located between the axial members as in Fig. C-22. The effects of this loading system on the rock structure was studied; and although the resulting stresses and displacements in the rock are less than those in the single-wall support design, there is no clear advantage to the concept. Furthermore, the concept suffers from the following.

1. Thick load-bearing plates and rock bolting are required for both walls.
2. Heat intercepts are required for both sides of the axial support; the rock wall and vacuum vessel inner face design is complicated for both walls; and warming pipes for the concrete liner and rock inner face are required for both walls.

3. The radial cooldown motions of the dewar must be accommodated at the dewar-axial strut interface.

With no clear advantage and a number or disadvantages, the concept is of questionable value.

B. A-Frame, Single-Wall, Low-Conductivity Strut Concept

One alternative to bridging the tunnel with support structure is to support all the loads off the outer wall with a low-conductivity strut or array of struts. A number of different designs of such a strut are possible. The design is shown in Fig. C-23. The basic elements of the design are an extruded member for attachment of the helium-vessel sections (weld plates), low-conductivity G-10CR or reinforced fiber glass polyester plates with heat intercepts, friction connection plates and bolts, and a bearing and support plate for attaching the strut to the rock wall.

The details of the design of the bolted through friction connections are standard practice[2,3] in machine design and only the results are discussed here. The basis for the design of the G-10CR reinforced epoxy plates is presented.

The plate design is based on a maximum stress criteria in accordance with the properties of G-10CR shown in Table C-VII.

TABLE C-VII

G-10CR MATERIAL PROPERTIES AS A FUNCTION OF TEMPERATURE

Temperature, K	Tensile Strength, MPa		Compressive Strength, MPa		Shear Strength, MPa
	F_1^t	F_2^{t*}	F_1^c	F_2^{c*}	F_{12}^*
295.0	415.1	395.0	-375.0	-355.2	178.0
76.0	824.6	787.0	-833.5	-795.0	398.0
4.0	861.8	862.1	-862.1	-821.0	411.0

1 indicates the warp direction
2 indicates the fill direction

*No data available for fill direction--these properties are assumed based on 95% of the warp directional values with shear value at one-half minimum compressive strength.

Seven conditions are assumed to apply. These are:

1. The reinforcing material is oriented such that the warp direction is aligned with the resultant applied load vector. The 1 and 2 axes define the warp and fill directions of the reinforcement as shown in Fig. C-24.

2. The average stress, in the St. Venant sense, is computed from the plane stress elasticity solution as

$$\sigma_x = -\frac{P_R}{A} + \frac{V_A xy}{I} \quad ,$$

$$\sigma_y = 0,$$

and

$$\tau_{xy} = \frac{V_A}{2I}\left(\frac{H^2}{4} - y^2\right) \quad ,$$

where

σ_x = normal stress in the x direction,
σ_y = normal stress in the y direction,
τ_{xy} = shear stress,
I = moment of inertia about the z axis,
A = cross sectional area,
P_R = the normal of x component of the applied loading, and
V_A = the shear or y component of the applied load.

3. Stresses are computed from this solution along lines x = constant at the locations of the heat intercepts and thus at known temperatures.

4. Transform the computed stress state to the principal lamina directions--σ_1, σ_2, τ_{12}.

5. The failure envelope is defined by

$$\sigma_1 \leq F_1^t \text{ or } \sigma_1 \leq F_1^c \quad ,$$

$$\sigma_2 \leq F_2^t \text{ or } \sigma_2 \leq F_2^c,$$

and

$$\tau_{12} \leq F_{12} \quad ,$$

where F_1^t, etc., are the strength data given in Table C-VII.

6. These are further restricted such that

$$\sigma_{1_{max}} < 0.95\ F_1^t \text{ or } \sigma_{1_{max}} \leq 0.95\ F_1^c,$$

$$\sigma_{2_{max}} < 0.95\ F_2^t \text{ or } \sigma_{2_{max}} \leq 0.95\ F_2^c,$$

and

$$\tau_{12_{max}} < 0.95\ F_{12} \quad .$$

7. The plate is stepped in width such that L1 will be of thickness T1 based on the temperature interpolated material properties from Table C-VII, and L2 of thickness T2, etc., see Fig. C-25.

Applying the above set of conditions leads to a set of equations for three thicknesses, where the largest t_1 must be taken, as

$$t_1 = \frac{1}{0.95\ F_1^t \text{ or } c} \left\{ \left(-\frac{P_R}{H} + \frac{12 V_A xy}{H^3} \right) \cos^2 \phi + \frac{12 V_A}{H^3} \left(\frac{H^2}{4} - y^2 \right) \cos \phi \sin \phi \right\} \quad ,$$

$$t_2 = \frac{1}{0.95\ F_1^{t\ \text{or}\ c}} \left\{\left(-\frac{P_R}{H} + \frac{12V_A xy}{H^3}\right) \sin^2 \phi - \frac{12V_A}{H^3}\left(\frac{H^2}{4} - y^2\right) \cos \phi \sin \phi\right\} ,$$

and

$$t_3 = \frac{12}{0.95\ F_{12}} \left\{-\left(-\frac{P_R}{H} + \frac{12V_A xy}{H^3}\right) \sin \phi \cos \phi + \frac{6V_A}{H^3} (\cos^2 \phi - \sin^2 \phi)\right\} ,$$

where

the $F_i^{t\ \text{or}\ c}$ is taken to be the tensile or compressive strength depending upon the final sign of the terms in the brackets.

Various configurations have been examined and are discussed. Figure C-26 shows the results of a sample calculation for the three thicknesses at the xz plane, Fig. C-24, that is computed for the various stress states vertically along the room-temperature end at 295 K for a 2.2-m-high, 1.5-m-long strut. The largest thickness in this case is 0.256 m at y = - 1.1 m and is determined by the fill direction strength criterion in the plane $\phi = 13.3^{\circ}$.

One obvious selection for strut heights is to have each strut support a helium vessel segment. For example, in the 13-segment concept, there would be 13 struts. By assuming 1.5-m-length struts and temperature stations as shown on Fig. C-24 for L1 = 0.435 m, L2 = 0.480 m, and L3 = 0.585 m, the required G-10CR volume can be computed for this concept. Table C-"III shows the results of this computation. A 2-m circumferential support spacing for 104 struts for each segment is used for these computations.

There is no obvious reason to have a separate strut for each segment. If the top and bottom six segments are supported by continuous struts 12.9 m in height with the central section supported by a single 18.2-m-long strut, then the results given in Table C-IX are obtained.

Computations of the remaining portions of the strut design are based on the cross section of Fig. C-25 and follow standard engineering design practice. All stainless steel parts were designed to a shear strength of 275 MPa and all bolts are assumed to be preloaded to 90% of their proof strength. Two rows of 38-mm-diam bolts on 175-cm centers are used on all connections. The joints are all designed as friction connections and a coefficient of friction of 0.6 was used between the G-10CR and stainless

TABLE C-VIII

G-10CR 13-SEGMENT SUPPORT STRUT MATERIAL REQUIREMENTS

Segment Number	Loading V_A MN	Loading P_R MN	Warp Orientation θ degrees	Strut Geometry H m	T1 m	T2 m	T3 m	Single Strut G-10 Volume m^3	Total G-10 Volume for all Segments m^3
1 & 7	46.4	11.0	± 13.3	2.2	0.076	0.080	0.256	0.486	101.1
2 & 8	46.4	12.6	± 15.2	1.7	0.098	0.118	0.420	0.586	121.9
3 & 9	46.4	14.4	± 17.2	1.8	0.090	0.105	0.370	0.551	114.6
4 & 10	46.4	18.8	± 22.1	2.0	0.075	0.087	0.290	0.488	101.5
5 & 11	46.4	24.8	± 28.1	2.3	0.058	0.072	0.220	0.433	90.1
6 & 12	46.4	31.9	± 34.5	2.9	0.039	0.052	0.167	0.404	84.0
13	0	207.0	0	18.2	0.014	0.015	0.032	0.58	60.3
									673.5

TABLE C-IX

G-10CR 3-SEGMENT SUPPORT STRUT MATERIAL REQUIREMENTS

Segment Number	Loading V_A MN	Loading P_R MN	Warp Orientation θ degrees	Strut Geometry H m	T1 m	T2 m	T3 m	Single Strut G10 Volume m^3	Total G-10 Volume for all Segments m^3
1 & 6	278.4	113.5	22.2	12.9	0.068	0.069	0.16	2.02	210.0
7 & 12	278.4	113.5	-22.2	12.9	0.068	0.069	0.16	2.02	210.0
13	0	207.0	0	18.2	0.014	0.015	0.032	0.58	60.3
								Total	480.3

steel. Table C-X shows the result of this design. The total strut material cost is about $14.0 million.

TABLE C-X

3-SECTION SUPPORT STRUT MATERIAL COSTS

Segment Numbers	G-10 Volume m^3	Estimated Stainless Steel Weld Plate Structure Volume m^3	Stainless Steel Connection Plate Volume m^3	Bearing Plate Volume m^3	No. of 38-mm High Strength SAE Grade 8 Bolts	Total Steel Volume m^3	G-10CR[b] Costs at \$8/kg $\$10^3$	Total Stainless Steel Costs $\$10^3$	Total Fastener Costs[a] $\$10^3$	Single Strut Cost $\$10^3$	Total Segment Costs 104 Struts Circumference $\$10^6$
1-6	2.02	0.52	0.433	0.16	592	1.11	32.4	19.3	11.8	63.5	6.6
13	0.58	0.73	0.612	0.23	406	1.57	9.3	27.2	8.3	44.8	4.7
7-12	2.02	0.52	0.433	0.16	592	1.11	32.4	19.3	11.8	63.5	6.6
										Total	17.9

[a]Fastener costs assumed to include all lengths of bolts plus nuts and washers at an average cost of \$20/fastener.

[b]Density for high glass content taken as 2 g/cm^3.

IV. THE WIRE-ROPE CABLE DESIGN AND ASSOCIATED SUPPORT CONCEPT

A. Design Considerations for a Load-Carrying Cable

Wire-rope design is a very complex process from a theoretical point of view. References 6 through 8 give some selected analyses of stresses of fairly complex designs, all of which have various restrictive assumptions that are necessary to obtain a solution. Perhaps the most observant statement comes from a discussion from Ref. 8, "... it has become quite evident to us over the years that wire-rope manufacture is an art, not a science." The increasing body of literature in the area will invalidate this observation. Structurally, a design of a conductor that is very flexible, yet self-supporting, is ideal for SMES application. For this reason the design of such a conductor has been investigated.

For a reference design of this nature, the following assumptions are made.

1. The cable is flexible enough that bending stresses in the unsupported region are negligible, and the cable takes on a true cylindrical shape.

2. The maximum stresses in the cable occur as it passes over the support where the bending moment can be calculated from

$$M = \frac{E_e I}{r} \quad ,$$

where

E_e = the equivalent cable modulus of elasticity,

r = the support radius, and

I = the moment of inertia an individual wire in the cable has about an axis through its centroid.

B. *Cable Statics*

Consider Fig. C-27 which shows the geometry involved and Fig. C-28 which shows a free body diagram of the element under its magnetic body loading, $p^{(B)}$, where $p^{(B)}$ is the force per unit length normal to the cable. From equilibrium, if the cable is flexible enough, the curve for a loading normal to the cable will be a portion of a circle; and the tension in the cable will be given by $T = p^{(B)}R$. The inflection point in the cable as it passes over the support is assumed to be at the point of contact with the support. Under load, the cable will wrap around the support and the maximum normal stress at the support caused by the tensile load plus bending over the support is

$$\sigma_{max} = \frac{p^{(B)}R}{A} + \frac{E_e c}{r} \quad ,$$

where

c = radius of the wires in the cable,

A = cross-sectional area of the cable, and

E_e = the cable equivalent modulus of elasticity.

If n is the number of wires in the cable, then $A = n\pi c^2$, and

$$\sigma_{max} = \frac{p^{(B)}R}{n\pi c^2} + \frac{E_e C}{r} \qquad \text{(C-34)}$$

This equation can be put into the form of a design equation as,

$$\frac{1}{R} c^3 - \frac{r}{R} \frac{\sigma_{max}}{E} c^2 + \frac{p^{(B)}r}{n\pi E_e} = 0 \qquad \text{(C-35)}$$

Now, incorporation of the geometric constraint on the arc length and support spacing S is such that

$$S = 2 (R + r) \sin \phi \ ,$$

where ϕ = the support half-angle. Equation(C-35) can then be written in terms of the geometry, S and ϕ, as

$$\frac{1}{R} c^3 - \left\{\frac{S}{2R \sin \phi} - 1\right\} \frac{\sigma_{max}}{E_e} c^2 + \frac{p^{(B)}r}{n\pi E_e} = 0 \ . \qquad \text{(C-36)}$$

As an example, a 50-kA conductor in a 4.2-T field can be considered, and the solution to Eq.(C-36) can be obtained with the following parameters.

$p^{(B)}$ = 210 kN/m

S = 2 m

R = 1.21 m

r = 0.2 m

$\phi = 45^{\circ}$

σ_{max} = 510 MPa

E_e = 62.1 GPa

Because Eq.(C-36) is cubic, the first positive pairs of real roots which are physically admissible occur for n = 373. As n is increased further, there are two possible values of the radius c that represent a physically admissible solution. The larger value of c represents the solution for which the maximum stress in Eq.(C-34) is dominated by the second term, that is, by bending, whereas for the smaller value of c, Eq.(C-34) is dominated by the membrane term.

The solution for n = 373 is that for which the bending contribution and membrane stresses are most nearly equal. For this case, 373 wires of 2.2-mm diameter would compose a suitable wire rope in keeping with the design assumptions.

Figures C-29 and C-30 show the two physically admissible solutions from Eq.(C-36). The analysis suffers several shortcomings. First, the realities of wire-rope manufacture may preclude making a cable of 373 wires or greater. This point needs more investigation. Second, the frictional losses associated with such a conductor are unknown and may be large. This question also needs further investigation, probably experimentally. Other materials also should be investigated for a potential load-carrying conductor design.

REFERENCES

1. F. D. JU, "On the Constraints for Castigliano's Theorem," Journal of the Franklin Inst. 292, 257-264 (1971).

2. J. E. Shigley, Mechanical Engineering Design, (McGraw-Hill, New York 1977).

3. J. E. Shigley, Machine Design, (McGraw-Hill, New York 1956).

4. G. P. Sendecky, Ed., Mechanics of Composite Materials, Composite Materials 2, (Academic Press, New York 1974).

5. C. C. Chamis, Ed., Composite Materials 8, Structural Design and Analysis, Part II, (Academic Press, New York, 1975).

6. G. A. Costello and R. E. Miller, "Lay Effect of Wire Rope," University of Illinois at Urbana-Champaign, Department of Theoretical and Applied Mechanics report #242 (October 1977).

7. G. A. Costello and J. W. Phillips, "Static Response of Stranded Wire Helical Springs," University of Illinois, Department of Theoretical and Applied Mechanics report #423 (January 1978).

8. W. L. Starkey and H. A. Cress, "An Analysis of Critical Stresses and Mode of Failure of a Wire Rope," J. Eng. Indus., Transactions of the ASME, pp. 307-311 (November 1959).

Fig. C-1. Basic dimensions and cross section of 13-segment vessel concept.

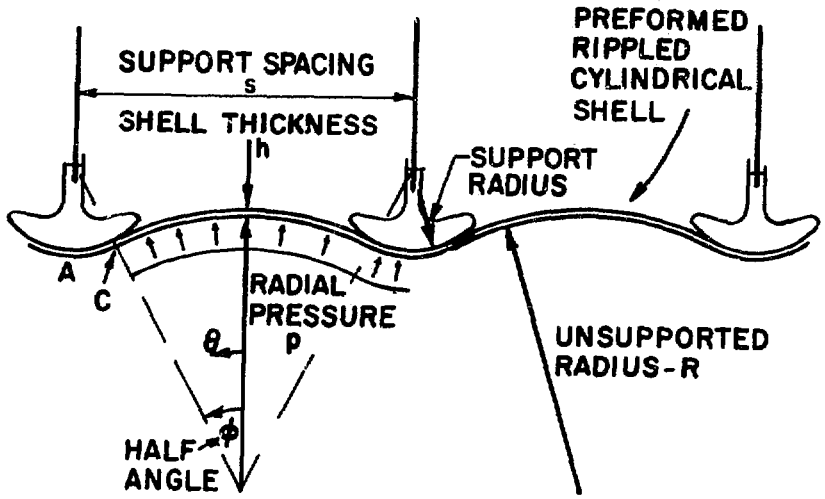

Fig. C-2. Geometry for a rippled shell design.

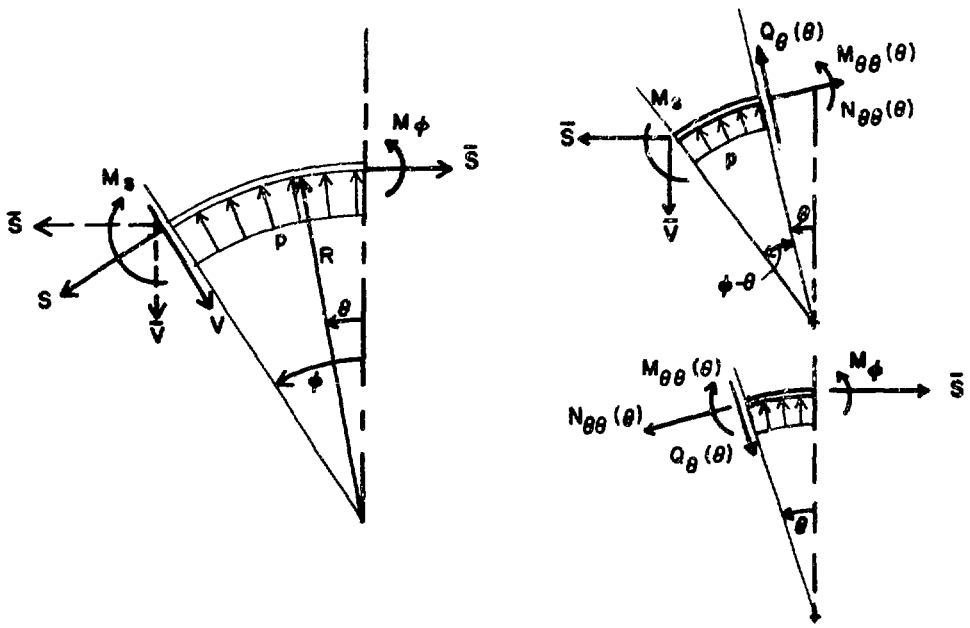

Fig. C-3. Free-body diagram for the shell equations.

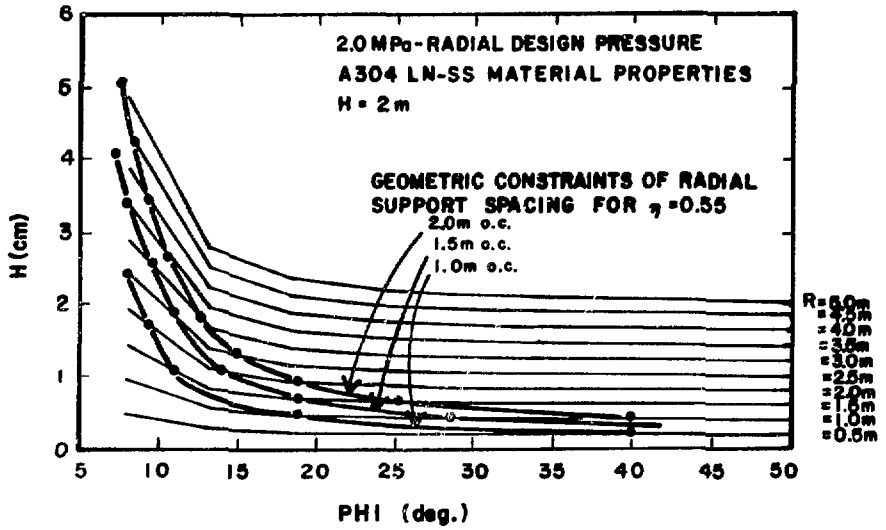

Fig. C-4. Shell thickness versus half-angle for r/R = 0.55.

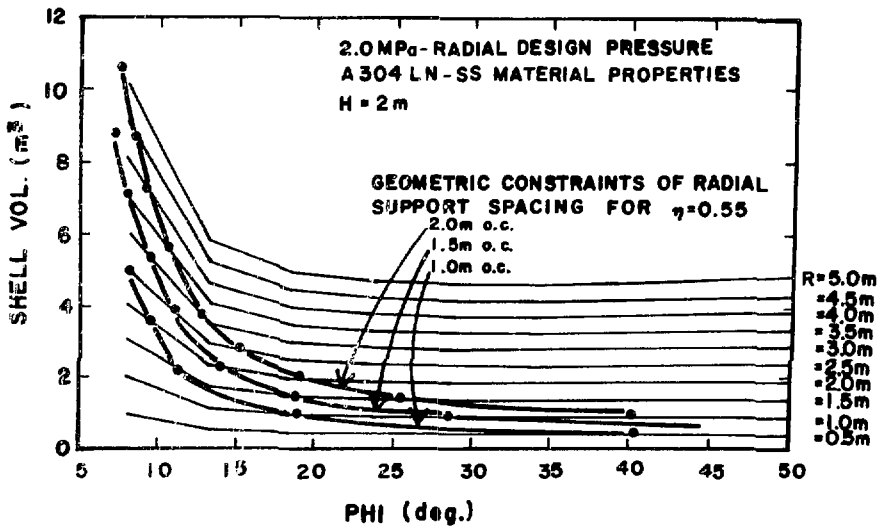

Fig. C-5. Shell volume versus half-angle for r/R = 0.55.

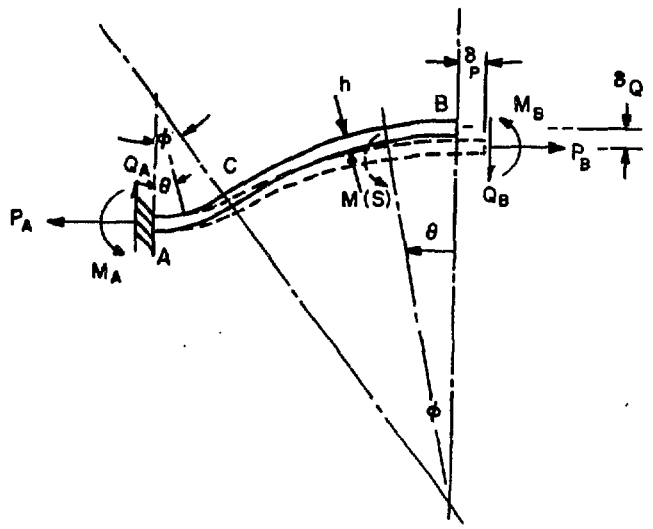

Fig. C-6. Free-body diagram for cooldown stress in the preformed shell wall.

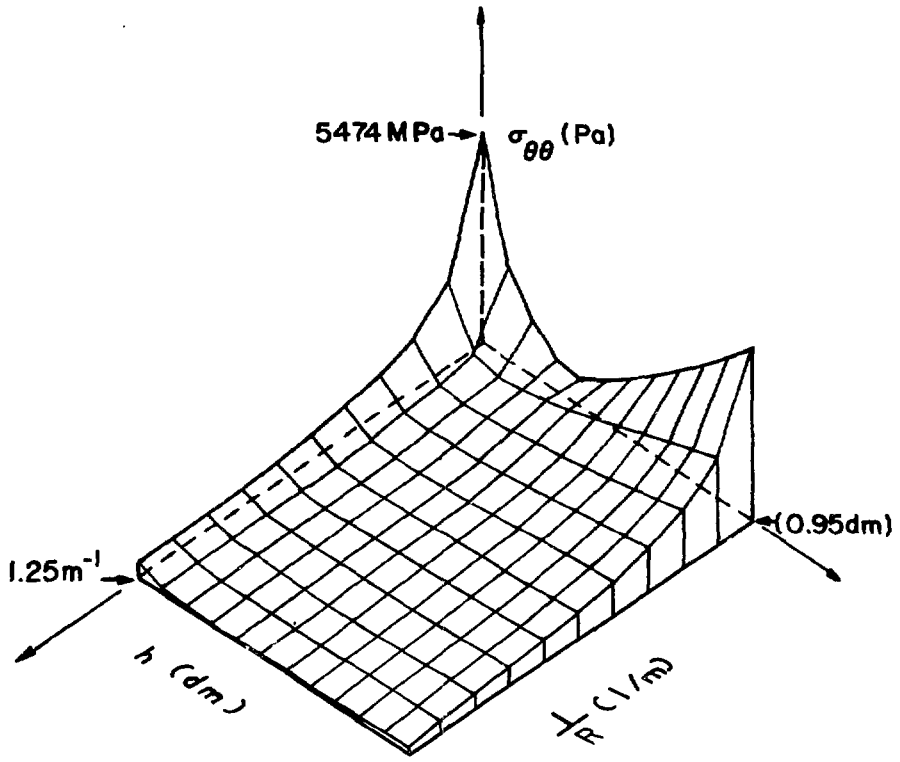

Fig. C-7. Hoop stress versus unsupported curvature versus thickness from Eq.(22).

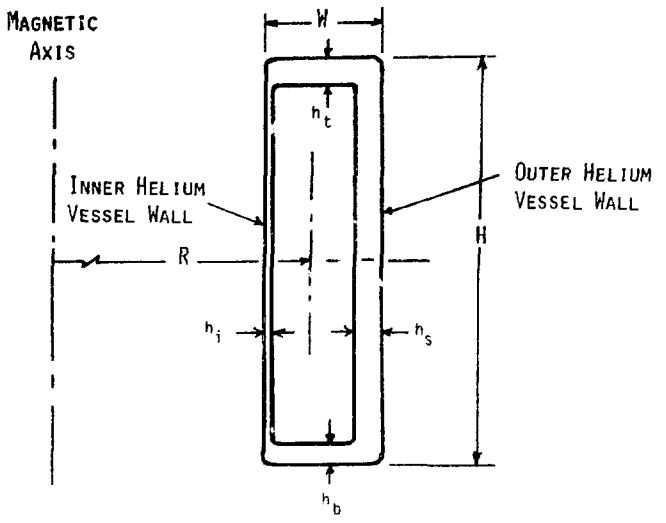

Fig. C-8. Typical dewar cross section.

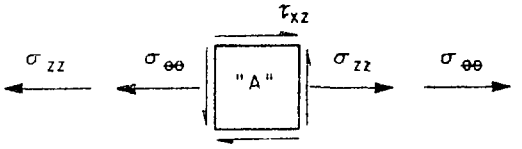

Fig. C-9. Differential element at position A.

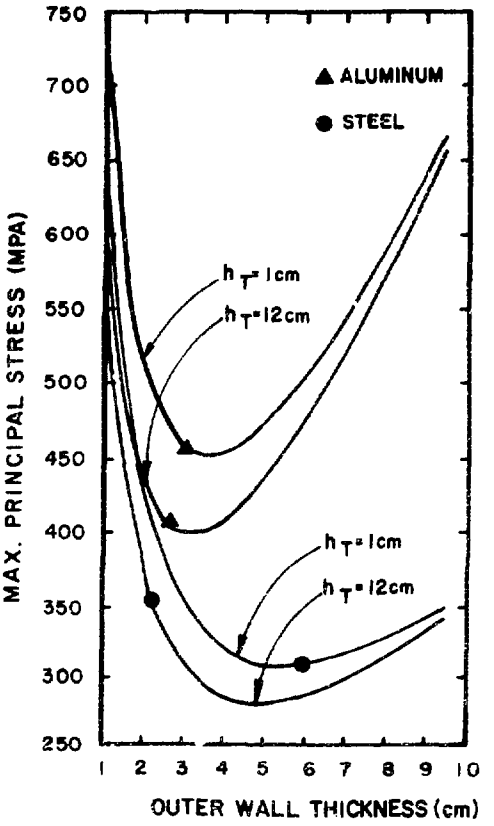

Fig. C-10. Maximum principal stress versus outer wall thickness for an aluminum and steel design.

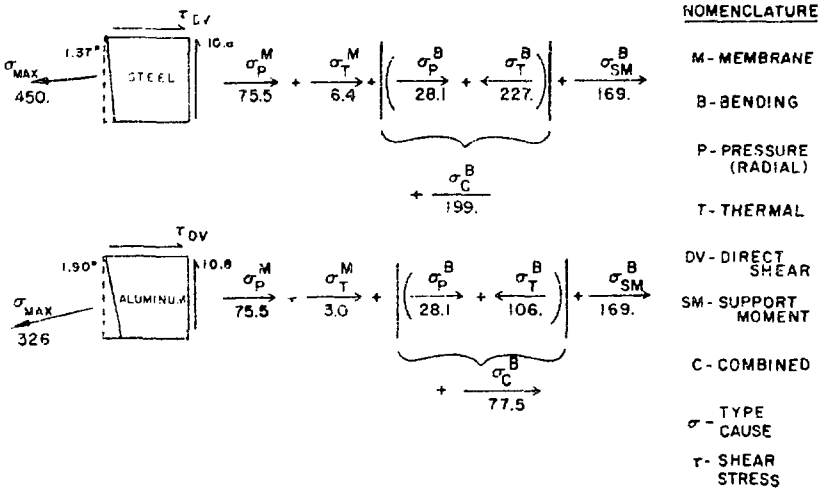

Fig. C-11. Comparison of the stress state in an aluminum and steel design at a point for a particular geometry.

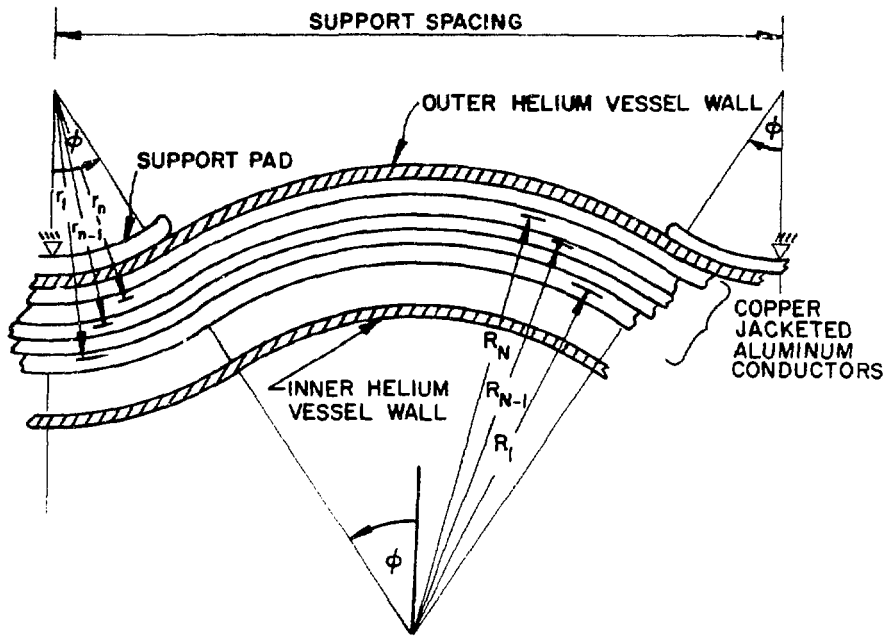

Fig. C-12. Horizontal cross section of the doubly curved box-beam vessel concept, treating the conductors as doubly curved beams.

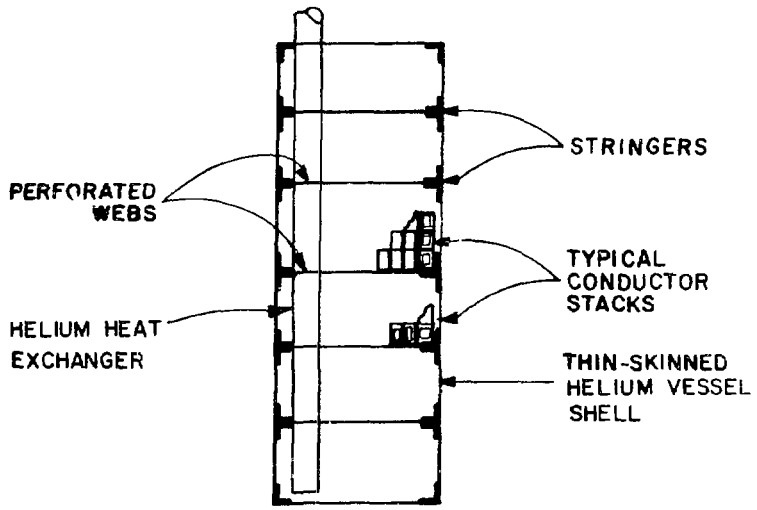

Fig. C-13. Typical vessel cross section for the box-beam concept.

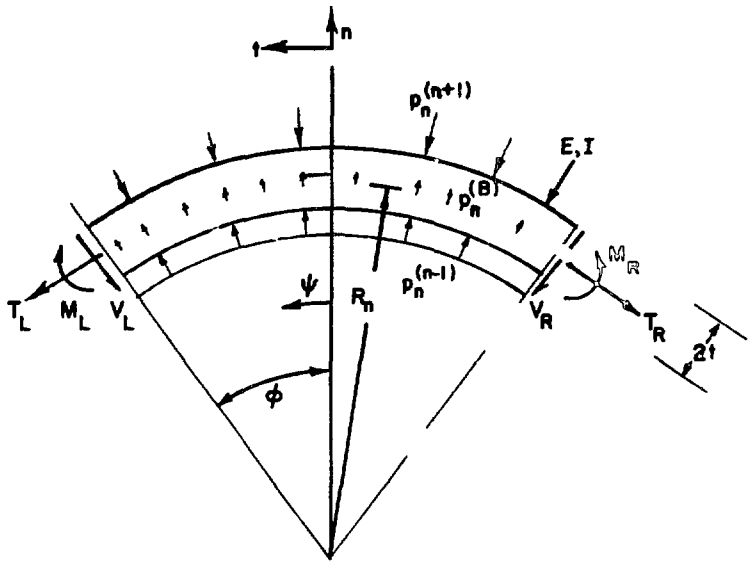

Fig. C-14. Unsupported region for nth copper clad conductor.

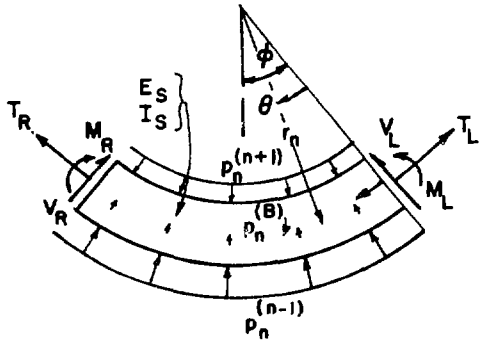

Fig. C-15. Supported region for nth copper clad conductor.

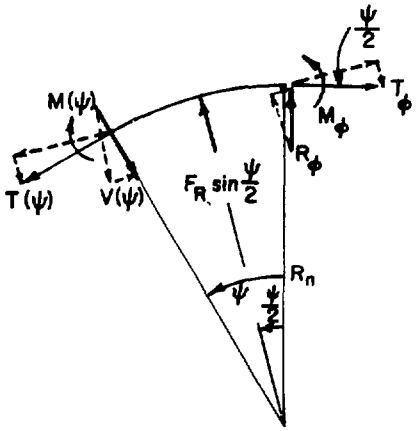

Fig. C-16. Free-body diagram from $\psi = 0$ to $\psi = \phi$ for the unsupported region.

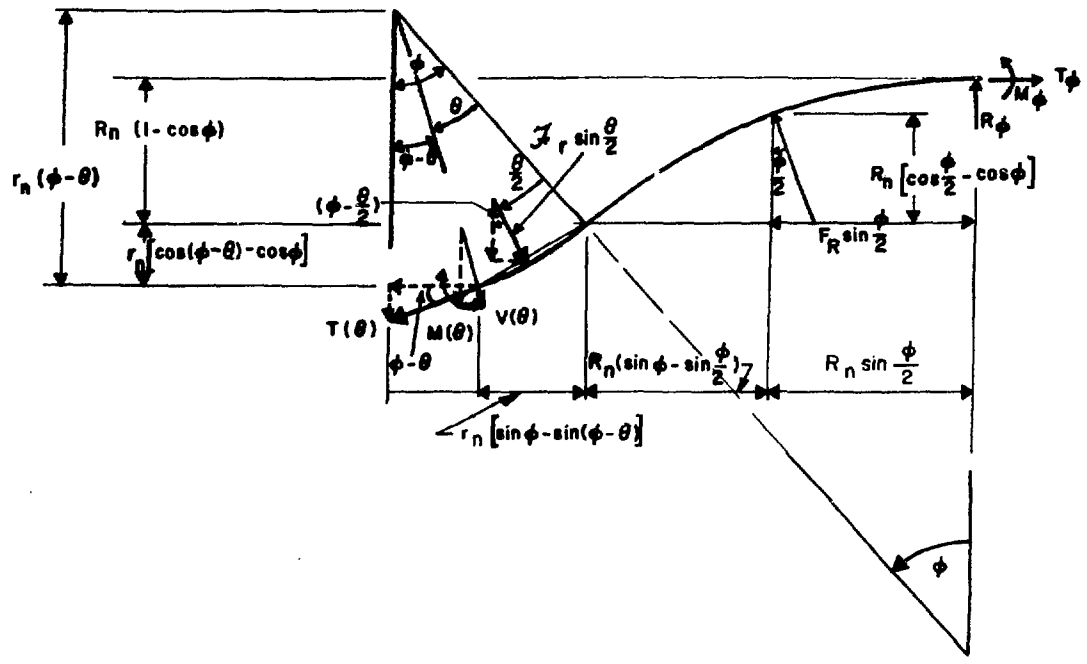

Fig. C-17. Free-body diagram from $\theta = 0$ to $\theta = \phi$ for the supported region.

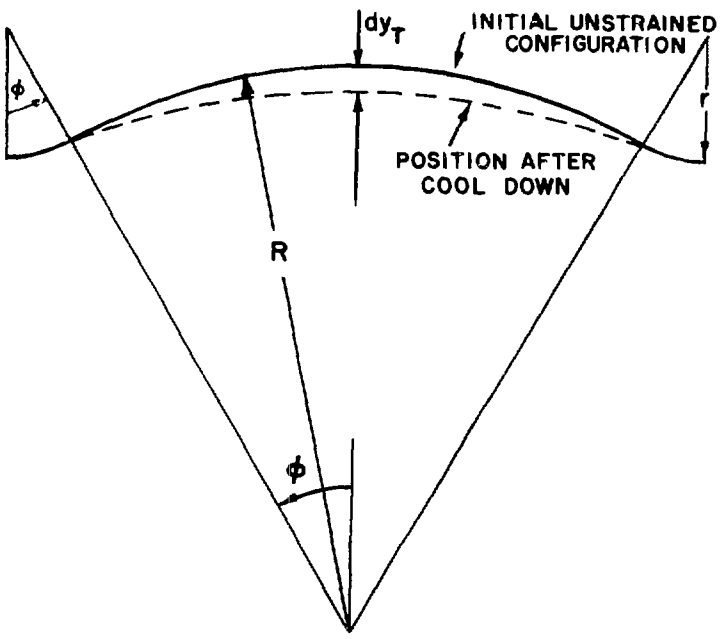

Fig. C-18. Kinematics of cooldown.

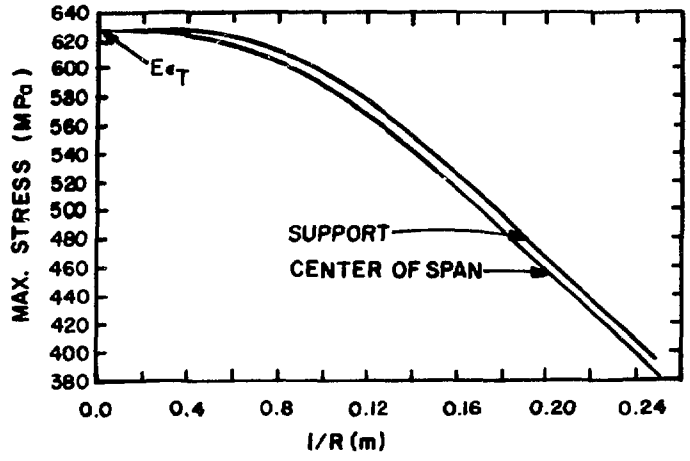

Fig. C-19. Cooldown stress for a shallow stiff vessel.

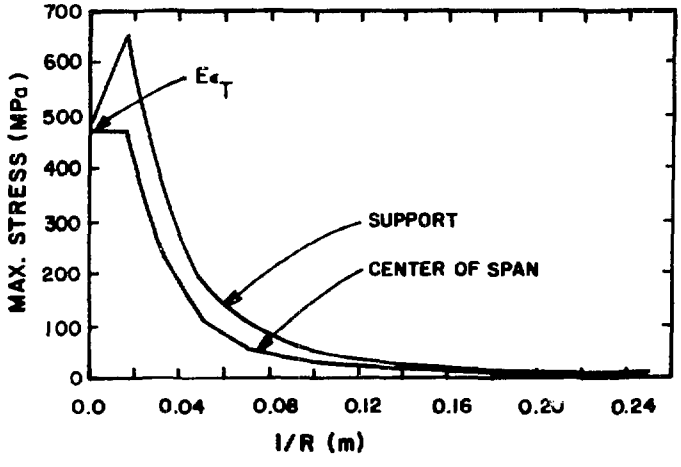

Fig. C-20. Cooldown stress in a flexible conductor.

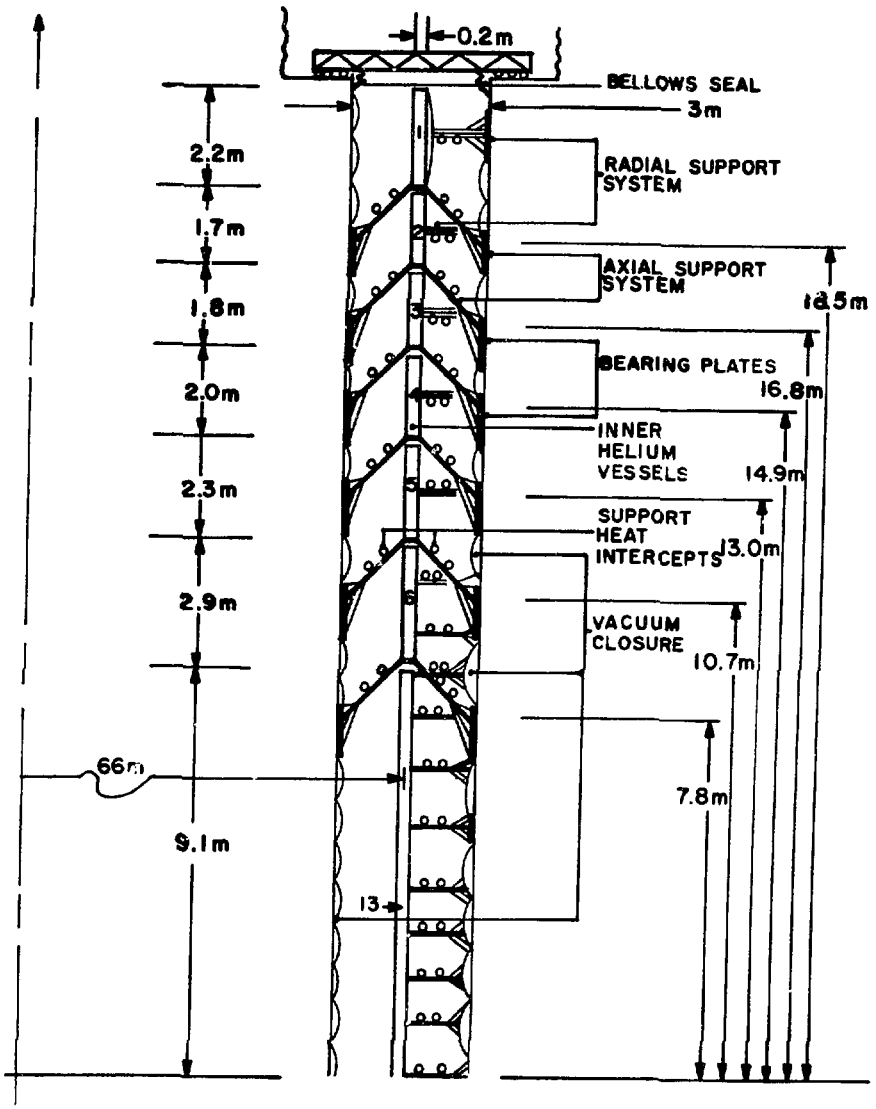

Fig. C-21. Basic cross section of the bridged-cavity concept.

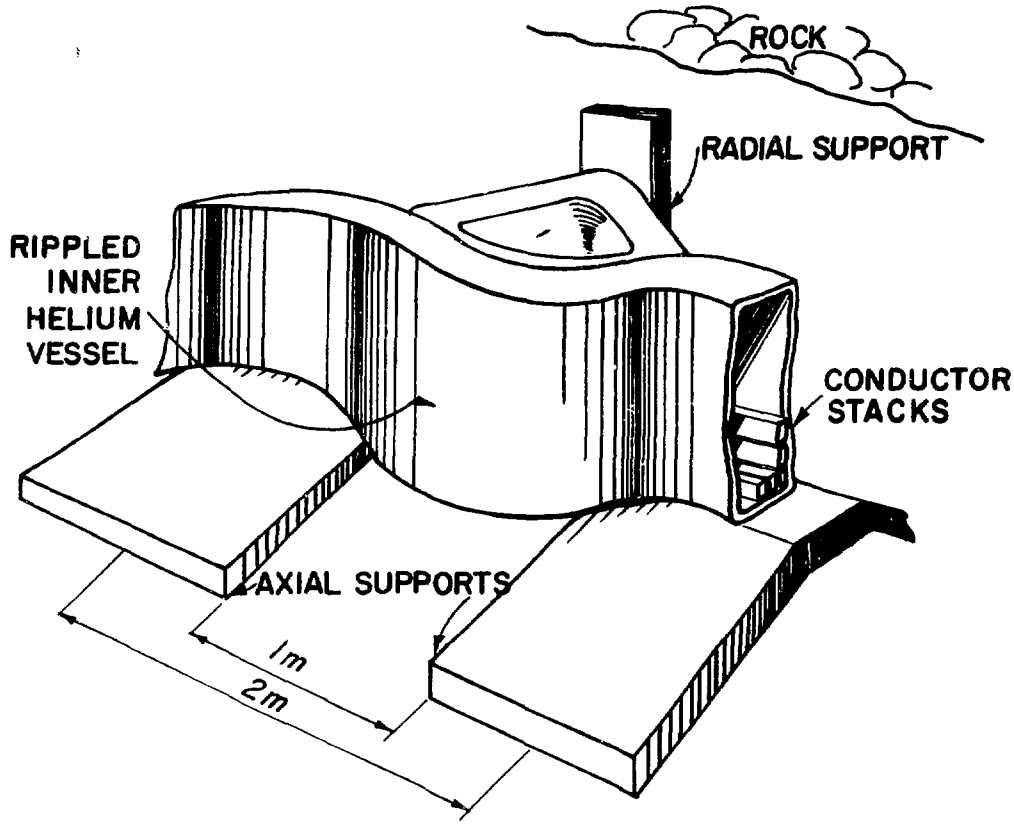

Fig. C-22. Bridged-cavity concept with separate radial and axial support systems.

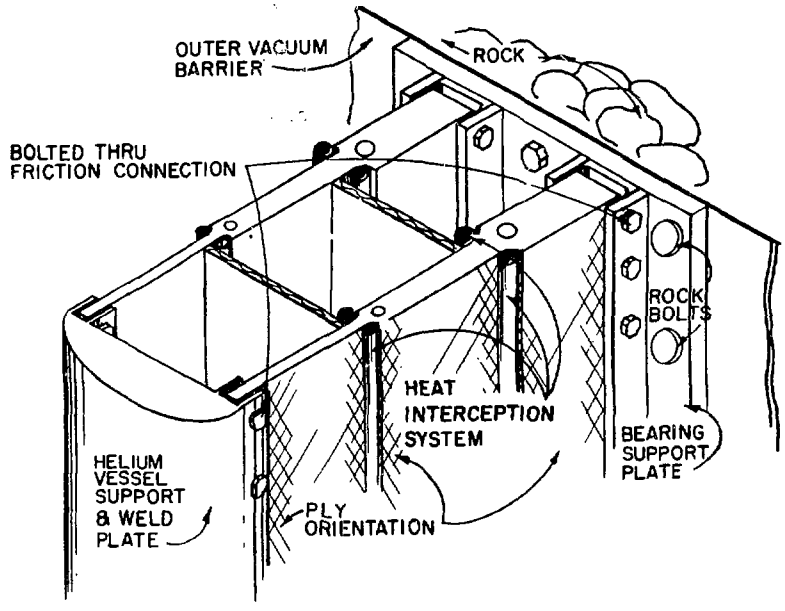

Fig. C-23. Low-thermal conductivity support components.

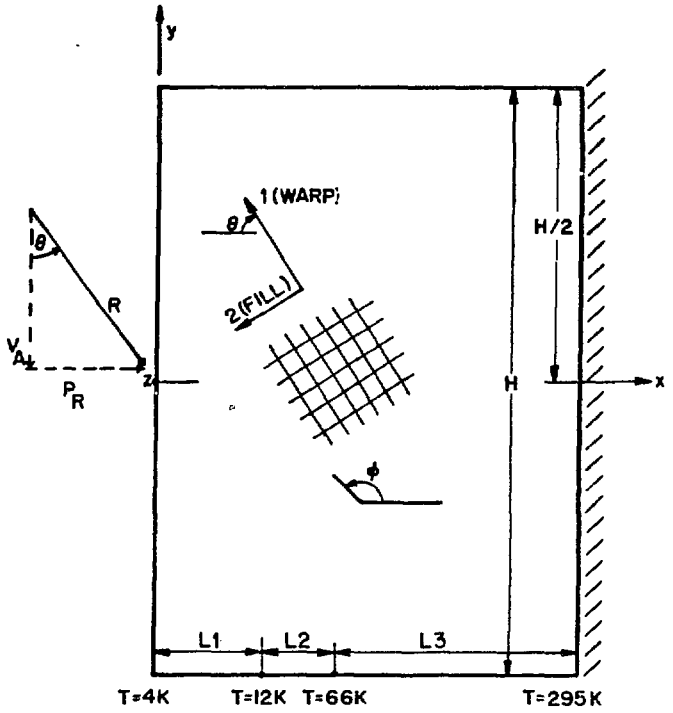

Fig. C-24. Geometry and variable definition for G-10 CR plate design.

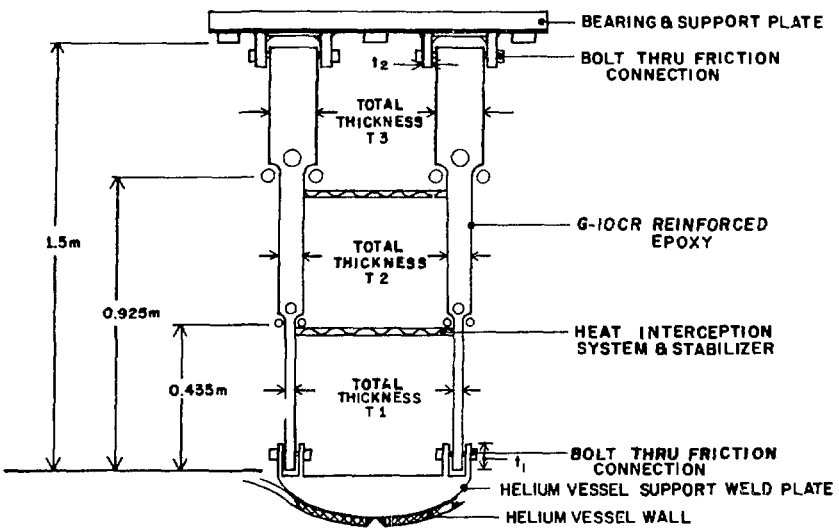

Fig. C-25. Strut cross section and variable definition.

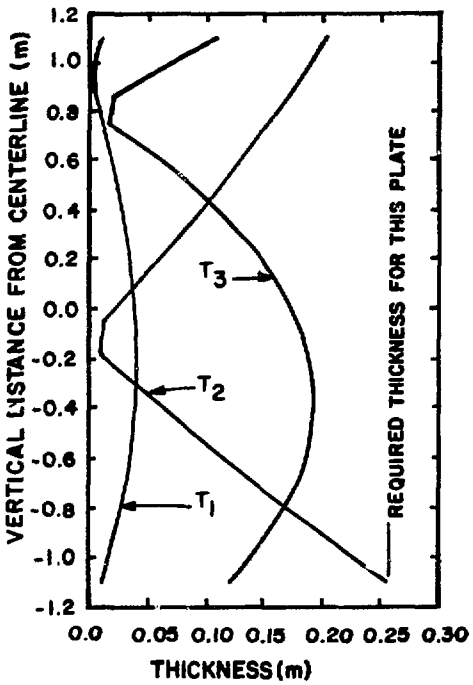

Fig. C-26. Typical results obtained from evaluating Eq. (34) at the room temperature end showing the strut thickness at y = 0 required to satisfy the calculated stress state at various positions along the y-axis.

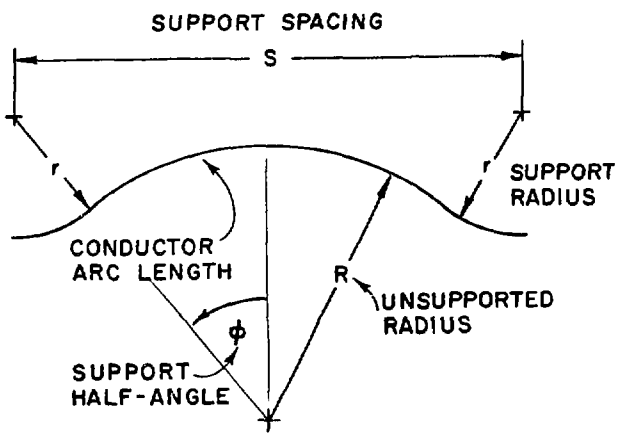

Fig. C-27. Geometry and variable definition for the wire-rope study.

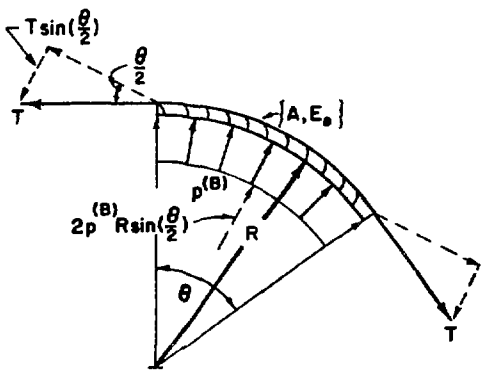

Fig. C-28. Free-body diagram of a flexible wire rope under magnetic loading.

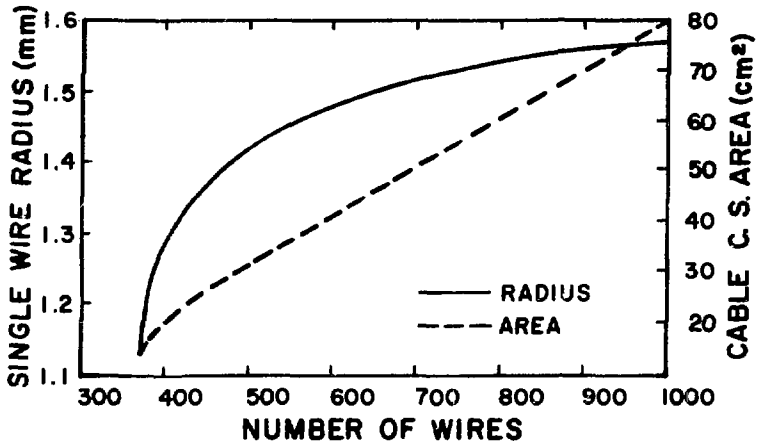

Fig. C-29. Single-wire radius and cable cross-sectional area from Eq.(37) as a function of the number of wires in the cable for a cable dominated by bending stress.

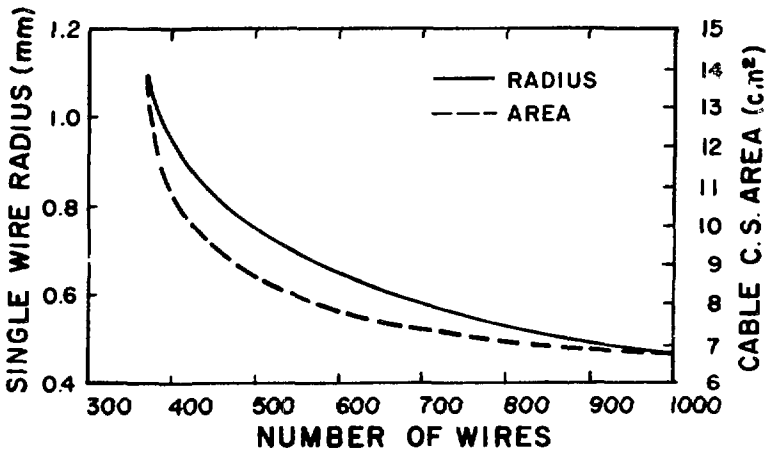

Fig. C-30. Single-wire radius and cable cross-sectional area from Eq.(37) as a function of the number of wires in the cable for a cable dominated by membrane stress.

☆ U.S. Government Printing Office: 1979 – 677–115/193